SAND2018-10770C

Model Reduction of Self-Repeating Structures and Applications to Metamaterial Modeling

Ryan Romeo
College of Engineering
University of Georgia
Athens, GA 30602
rromeo@uga.edu

Ryan Schultz
Structural Dynamics Department
Sandia National Laboratories[1]
Albuquerque, NM 87185
rschult@sandia.gov

Abstract
The dynamic behavior of metamaterials and metastructures is often modeled using finite elements; however, these models can become quite large and therefore computationally expensive to simulate. Traditionally, large models are made smaller using any of the array of model reduction methods, such as Guyan or Craig-Bampton reduction. The regularized nature of metamaterials makes them excellent candidates for reduced-order modeling because the system is essentially comprised of a repeating pattern of unit cell components. These unit cell components can be reduced and then assembled to form a reduced-order system-level model with equivalent dynamics. The process is demonstrated using a finite element model of a 1-D axially vibrating metamaterial bar using Guyan, SEREP, and Craig-Bampton reduction methods. The process is shown to provide substantial reduction in the time to simulate the dynamic response of a representative metamaterial while maintaining the dynamics of the system and resonators.

Keywords: metamaterials, self-repeating structures, reduced-order modeling, component mode synthesis

1 Introduction

Capturing the small and large-scale features of structures often results in a finite element model (FEM) that is large and therefore time consuming to run. To combat this, reduced-order modeling (ROM) techniques are used to condense the number of degrees of freedom and create a nearly dynamically equivalent FEM with fewer elements [1]. In this paper, a technique is proposed to take advantage of the nature of self-repeating structures—objects whose models can be divided into a number of identical groups of elements—and reduce the computational expense for obtaining a reduced-order model. One such type of structure seeing recent attention is metamaterials.

Metamaterials are structures which have a number of attached parasitic masses, called metaresonators. These resonators behave as tuned mass dampers, where they absorb kinetic energy from the vibrational response of the parent structure when it resonates near the natural frequencies of the attached masses, therefore decreasing the central structure's resonance response at those frequencies [2]. Metamaterials are typically designed to have a pattern of metaresonators attached along a homogeneous structure; as such, they often have self-repeating geometries.

The process presented here seeks to reduce the time to obtain a reduced-order model for self-repeating structures such as metamaterials. Because these structures can be grouped into identical sets of elements, called unit cells, it should be possible to take one of these unit cell element groups, apply a reduction, and then combine the result with copies of itself to make a full-sized assembly. As this assembly is comprised of a copy of ROM of a single unit cell, the overall computational time is greatly reduced compared to the computational time of running the original, full FEM.

[1] Sandia National Laboratories is a multimission laboratory managed and operated by National Technology and Engineering Solutions of Sandia, LLC., a wholly owned subsidiary of Honeywell International, Inc., for the U.S. Department of Energy's National Nuclear Security Administration under contract DE-NA0003525.

2 Reduced-Order Modeling Techniques Applied to Self-Repeating Structures

Modern finite element models can become quite large (i.e., millions of degrees of freedom) when trying to achieve an accurate representation of a physical object. Model reduction significantly expedites the time to obtain a solution; however, for considerably large FEMs, the reduction itself can become quite computationally expensive and complicated. The process described herein seeks to reduce the time spent in the reduction step, thus further decreasing the overall solution time.

2.1 Fundamental Process

The first step in the process is to divide the metamaterial finite element model into *m* identical groups of elements. One such group is then chosen to become the unit cell, or copy cell. The unit cell is then isolated from the rest of the model via its system property (i.e., mass and stiffness) matrices. A model reduction method is applied to these unit cell matrices, resulting in a ROM for the unit cell. Finally, the ROM cell is copied *m-1* times to form the reduced, full-sized assembly. A depiction of this process is provided in **Fig. 1**. System-level boundary conditions should not be applied to the model until the reduced, copied assembly has been obtained.

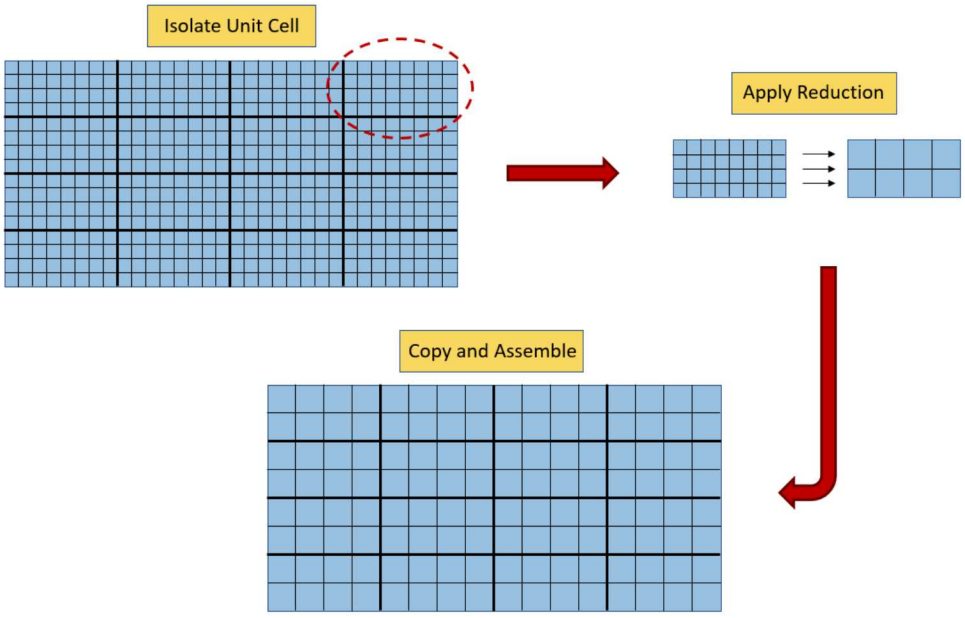

Figure 1. Visualization of the reduction process for self-repeating structures.

2.2 Reduced-Order Modeling Techniques

Three types of model reduction techniques will be explored in this paper: Guyan condensation, System Equivalent Reduction Expansion Process (SEREP), and Craig-Bampton Reduction (CBR). Generally, a reduction method takes the full *n*-set of finite element degrees of freedom and splits them into two subsets—the *a*-set (active) and *d*-set (deleted)—written as

$$x_n = \begin{Bmatrix} x_a \\ x_d \end{Bmatrix}. \quad (1)$$

The active set, x_a, contains those degrees of freedom which are determined necessary to accurately represent the dynamics of the system, whereas the deleted set, x_d, contains those DOF to be disregarded. The active set DOFs remain in the ROM. Next, a transformation matrix, $T_{n,a}$, is sought which directly relates the *n*-set DOFs with those in the *a*-set:

$$x_n = T_{n,a} x_a. \quad (2)$$

The reduced mass and stiffness matrices, M_a and K_a, are then obtained by

$$M_a = T_{n,a}^T M_n T_{n,a}, \quad (3)$$
$$K_a = T_{n,a}^T K_n T_{n,a}, \quad (4)$$

where M_n and K_n are the mass and stiffness matrices from the original finite element model, respectively.

In the technique presented, the reduced matrices are obtained for the unit cell and assembled to its copies using the same principle for assembling finite element model matrices; an example is shown in **Fig. 2**. Specifically, the *M* and *K* sets of reduced matrices and their respective copies are assembled to form two system-level block diagonal matrices. The main diagonal entries corresponding to the DOF connections between two connecting cells are added together, and the associated off-diagonal terms are changed accordingly. In the diagram, this is shown as the corners of each matrix overlapping.

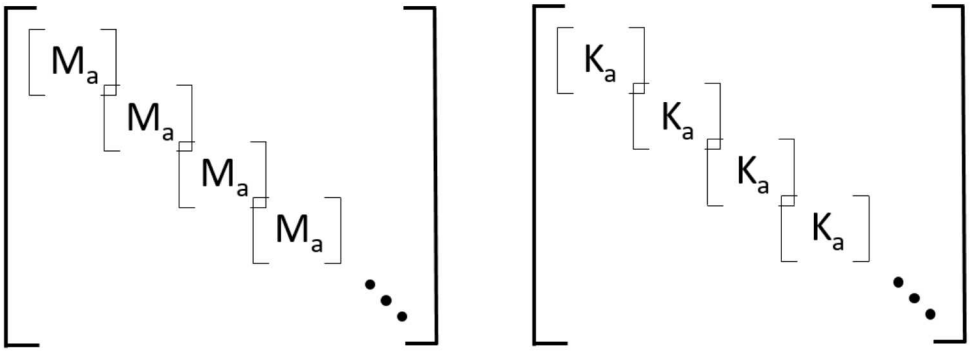

Figure 2. Depiction of the assembly of the reduced M and K matrices.

2.2.1. Guyan Reduction

Guyan reduction, also known as Guyan or static condensation, is one of the oldest and most well-known model reduction techniques. It involves manipulating the static force equation such that the degrees of freedom are rearranged according to the active and deleted sets [3], expressed as

$$F_n = K_n x_n, \tag{5}$$

$$\begin{Bmatrix} F_a \\ F_d \end{Bmatrix} = \begin{bmatrix} K_{aa} & K_{ad} \\ K_{da} & K_{dd} \end{bmatrix} \begin{Bmatrix} x_a \\ x_d \end{Bmatrix}. \tag{6}$$

Here, K_{aa} contains the stiffnesses at and between all active degrees of freedom, K_{ad} and K_{da} contain the stiffness connections between active and deleted sets ($K_{ad} = K_{da}^T$), K_{dd} contains the stiffnesses and connections between all deleted degrees of freedom, and F_a and F_d contain the forces acting on the active and deleted DOFs, respectively. Next, the lower partition is taken and F_d is assumed zero (i.e., no forces act on a deleted DOF), yielding:

$$K_{da} x_a + K_{dd} x_d = 0,$$

$$x_d = -K_{dd}^{-1} K_{da} x_a. \tag{7}$$

Substituting **Eq. (7)** into the top partition of **(6)** leads to

$$F_a = (K_{aa} - K_{ad} K_{dd}^{-1} K_{da}) x_a, \tag{8}$$

where the system is now reduced in that its static equilibrium is expressed only with the active DOFs—the set of relevant DOFs has been *condensed* to exclude the deleted set. Thus, **Eq. (7)** can be used to satisfy **Eq. (2)** and determine the Guyan transformation matrix, T_G:

$$\begin{Bmatrix} x_a \\ x_d \end{Bmatrix} = \begin{bmatrix} I_{aa} \\ -K_{dd}^{-1} K_{da} \end{bmatrix} x_a = T_G x_a, \tag{9}$$

where I_{aa} is the Identity matrix with dimensions a by a. The reduced mass and stiffness matrices can then be determined according to **Eqs. (3-4)**.

It should be noted that the traditional Guyan reduction technique presented above does not account for mass-inertial effects on the system resulting from the deleted DOFs; thus, an improved Guyan reduction has been developed to combat this for situations where such considerations are critical [4]. The improved Guyan transformation, T_G^*, is defined as

$$T_G^* = T_G + \begin{bmatrix} 0 & 0 \\ 0 & K_{dd}^{-1} \end{bmatrix} M_n T_G M_a^{-1} K_a, \tag{10}$$

where M_n is the n-set mass matrix partitioned according to K_n in **Eq. (6)**, and M_a and K_a are the traditional Guyan-condensed mass and stiffness matrices.

2.2.2. System Equivalent Reduction Expansion Process

The SEREP transformation operates using a modal space projection between the reduced a-set and the full n-set [4]. The modes of the FEM are computed, and the mode shapes, U_n, are partitioned based on the active and deleted DOFs:

$$x_n = U_n p, \tag{11}$$

$$\begin{Bmatrix} x_a \\ x_d \end{Bmatrix} = \begin{bmatrix} U_a \\ U_d \end{bmatrix} p, \tag{12}$$

where U_a and U_d are the sets of mode shapes corresponding to the active and deleted DOFs and p is the corresponding set of modal-space degrees of freedom. The top partition of **Eq. (12)** can be manipulated and then inserted into **Eq. (11)** to obtain the SEREP transformation matrix as in **Eq. (2)**:

$$p = U_a^{\dagger} x_a,$$

$$x_n = U_n U_a^{\dagger} x_a = T_S x_a. \tag{13}$$

Because U_a is not necessarily square, the generalized inverse is taken, denoted by $\circ^{\dagger}$.

2.2.3. Craig-Bampton Reduction

Craig-Bampton reduction is not a traditional model reduction method; rather, it is a component-mode synthesis technique which acts as a reduction method [5]. As a result, it is implemented differently than the previously mentioned techniques. The method begins by first identifying the components that will be connected. For each component, the set of n degrees of freedom is split into two sets—the i-set (interior) and the b-set (boundary):

$$x_{CB}^{(s)} = \begin{Bmatrix} x_i^{(s)} \\ x_b^{(s)} \end{Bmatrix}, \tag{14}$$

where x_{CB} is the Craig-Bampton partitioned set of DOFs, x_i and x_b represent the interior and boundary DOF sets, and $\circ^{(s)}$ denotes that the associated variable differs based on the component (substructure) it represents. The boundary set contains the DOFs which will overlap with those of another component to connect them together, and the interior set contains the remaining DOFs. Similarly to **Eq. (6)**, the original mass and stiffness matrices can then be arranged according to **Eq. (14)**:

$$\widehat{M}_{CB}^{(s)} = \begin{bmatrix} \widehat{M}_{ii}^{(s)} & \widehat{M}_{ib}^{(s)} \\ \widehat{M}_{bi}^{(s)} & \widehat{M}_{bb}^{(s)} \end{bmatrix}, \tag{15}$$

$$\widehat{K}_{CB}^{(s)} = \begin{bmatrix} \widehat{K}_{ii}^{(s)} & \widehat{K}_{ib}^{(s)} \\ \widehat{K}_{bi}^{(s)} & \widehat{K}_{bb}^{(s)} \end{bmatrix}. \tag{16}$$

The constraint modes, $\widehat{\Psi}_{ib}^{(s)}$, of each component are computed next. The constraint modes are the resulting static deformation of the given component when one of the b-set degrees of freedom is subjected to a unit displacement while the remaining coordinates in the boundary set are restrained and the DOFs in the i-set are left unforced. This is given as

$$\widehat{\Psi}_{ib}^{(s)} = -\widehat{K}_{ii}^{-1} \widehat{K}_{ib}. \tag{17}$$

Now the fixed-interface modes, $\widehat{\Phi}_{ii}$, of each component are determined. These are the mode shapes that result from solving the eigenvalue problem for each component while restraining x_b, written as

$$\left[\widehat{K}_{ii}^{(s)} - \omega_{(s)}^2 \widehat{M}_{ii}^{(s)}\right]\left\{\widehat{\Phi}_{ii}^{(s)}\right\} = 0, \tag{18}$$

noting that here the resulting eigenvalues, ω, are not pertinent and can be disregarded.

It is at this point when the reduction can be implemented; this occurs by choosing the desired modes that contain the relevant dynamic information pertinent to the analysis which the reduced model should contain. The columns of $\widehat{\Phi}_{ii}$ contain the *i* number of interior modes of the given component. The modes desired to be used can be chosen by removing the corresponding columns from $\widehat{\Phi}_{ii}$ and using them to form $\widehat{\Phi}_{ia}$, where *a* is the number of reduced-set modes. Now, the Craig-Bampton transformation matrix, $\hat{T}_{CB}$, is assembled for each component as

$$\hat{T}_{CB}^{(s)} = \begin{bmatrix} \widehat{\Phi}_{ia}^{(s)} & \widehat{\Psi}_{ib}^{(s)} \\ 0 & I_{bb} \end{bmatrix}, \tag{19}$$

where I_{bb} is the *b* by *b* Identity matrix. Using **Eqs. (3-4)**, the componentwise mass and stiffness matrices can be transformed into CB coordinates:

$$M_{CB}^{(s)} = \hat{T}_{CB}^{(s)^T} \widehat{M}_{CB}^{(s)} \hat{T}_{CB}^{(s)}, \tag{20}$$

$$K_{CB}^{(s)} = \hat{T}_{CB}^{(s)^T} \widehat{K}_{CB}^{(s)} \hat{T}_{CB}^{(s)}. \tag{21}$$

Next, the Component Coupling Matrix, *S*, is formed. This is a Boolean matrix that relates the physical-space coordinates, x_{CB}, and the coordinate space used for the CB transformation, η_{CB}, by the relationship $x_{CB} = S \cdot \eta_{CB}$. An example is provided for a 3-component bar of 1-D elements:

$$\begin{Bmatrix} x_a^{(1)} \\ x_{b,R}^{(1)} \\ x_a^{(2)} \\ x_{b,L}^{(2)} \\ x_{b,R}^{(2)} \\ x_a^{(3)} \\ x_{b,L}^{(3)} \end{Bmatrix} = \begin{bmatrix} 1 & 0 & 0 & 0 & 0 \\ 0 & 0 & 0 & 1 & 0 \\ 0 & 1 & 0 & 0 & 0 \\ 0 & 0 & 0 & 1 & 0 \\ 0 & 0 & 0 & 0 & 1 \\ 0 & 0 & 1 & 0 & 0 \\ 0 & 0 & 0 & 0 & 1 \end{bmatrix} \begin{Bmatrix} \eta_{CB}^{(1)} \\ \eta_{CB}^{(2)} \\ \eta_{CB}^{(3)} \\ u_b^{(1)} \\ u_b^{(2)} \end{Bmatrix}.$$

Here, *L* and *R* denote the left and right boundary DOF sets, $\eta_{CB}^{(j)}$ contains the CB-transformed interior degrees of freedom of the *j*'th component, and $u_b^{(k)}$ is the set of boundary DOFs in CB coordinates contained in the *k*'th interface between components.

The reduced mass and stiffness matrices in Craig-Bampton space for the full assembly are formed by creating a block diagonal of the component matrices:

$$\bar{M} = \begin{bmatrix} M_{CB}^{(1)} & \cdots & 0 \\ \vdots & \ddots & \vdots \\ 0 & \cdots & M_{CB}^{(m)} \end{bmatrix}, \tag{22}$$

$$\bar{K} = \begin{bmatrix} K_{CB}^{(1)} & \cdots & 0 \\ \vdots & \ddots & \vdots \\ 0 & \cdots & K_{CB}^{(m)} \end{bmatrix}, \tag{23}$$

where *m* is the total number of components. The reduced physical-space system matrices are then

$$M = S^T \bar{M} S, \tag{24}$$

$$K = S^T \bar{K} S, \tag{25}$$

and the eigenanalysis of the reduced assembly can be performed:

$$\left[K - \omega_j^2 M\right]\{U_j\} = 0. \tag{26}$$

Now, $\overline{U}_{CB}$ is defined as the set of mode shapes in reduced physical coordinates and is found by horizontally concatenating U_j for all j modes. These ROM shapes can be dissected into

$$\overline{U}_{CB} = \begin{Bmatrix} U_a^{(1)} \\ U_a^{(2)} \\ \vdots \\ U_a^{(m)} \\ U_b \end{Bmatrix}, \tag{27}$$

where $U_a^{(j)}$ contains a modes of the j'th component's reduced set of interior DOFs and U_b contains a modes for the boundary set degrees of freedom among all components. Finally, the expanded mode shapes, U_{CB}, are determined by performing the following operations on the reduced mode shapes:

$$U_{CB} = \begin{bmatrix} \widehat{\Phi}_{ia}^{(1)} U_a^{(1)} + \widehat{\Psi}_{ib}^{(1)} U_b^{(1)} \\ U_b^{(1)} \\ \vdots \\ \widehat{\Phi}_{ia}^{(m)} U_a^{(m)} + \widehat{\Psi}_{ib}^{(m)} U_b^{(m)} \\ U_b^{(m)} \end{bmatrix}, \tag{28}$$

where the superscript of U_b denotes the component by which its rows should be used (e.g., if the superscript is 2, then the rows of U_b corresponding to the boundary degrees of freedom of the second component should are to be taken). It should be noted that the majority of boundary DOFs will be included in two different subscripted U_b partitions due to the overlapping of interface degrees of freedom between conjoined components.

3 Results from Finite Element Analysis

To demonstrate the validity and examine the effectiveness of the unit cell reduction technique, a simple finite element model of a metamaterial structure is created. Frequency response functions (FRFs) of the FEM and ROMs are generated to compare reduction accuracy, and the frequency response assurance criterion (FRAC) is used to quantify the accuracy. The FRAC between two given FRF curves is computed as

$$FRAC = \frac{|H_{ROM} H_{FEM}^{*T}|^2}{|H_{ROM} H_{ROM}^{*T}| \cdot |H_{FEM} H_{FEM}^{*T}|}, \tag{29}$$

where H_{ROM} and H_{FEM} are the discrete transfer functions for the ROM and FEM and $\circ^{*T}$ denotes the Hermitian operator [6]. The FRAC ranges from 0 (no resemblance) to 1 (perfect match). For all cases, the FRF represents the response at the right end (5001st DOF) due to an input force at the left end (1st DOF), and the FRF magnitudes are presented in acceleration/force with units of $\frac{m/s^2}{N}$.

3.1 Model Description

The finite element model is developed using MATLAB and is formulated as a 1-dimensional axially vibrating bar. The bar is divided into 5,000 elements—to obtain many modes and a large DOF count for demonstrating the effects of the reduction—and a total of 10 resonators are attached to the bar to simulate the dynamic response of metamaterials. The bar is divided into 10 identical groups of 500 elements each, and one metaresonator is attached to the central DOF in each cell, each having a mass of 0.5% of the bar's total mass. Springs are attached to the left and right-most ends of the model, and their spring constants are varied to approximate free and fixed conditions (e.g., a spring stiffness near zero leads to an effectively free boundary condition). The metaresonators are implemented so that they have the same natural frequency of 20 kHz. The bar is 15.24 cm in length, has a solid square cross section with side lengths of 1.27 cm, and has an elastic modulus of $2.9 \cdot 10^5$ psi (ABS plastic). A diagram depicting a sparser FEM of the same configuration is provided in **Fig. 3**. Additionally, the first five mode shapes of the bar are plotted in **Fig. 4**, and the FRF of the FEM is shown in **Fig. 5**. Both are for fixed-free boundary conditions.

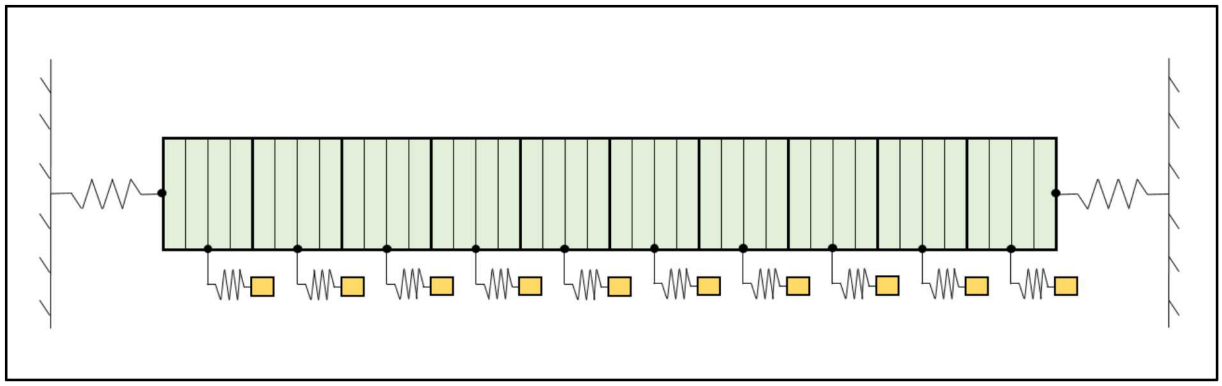

Figure 3. Diagram similar to the finite element model used for analysis.

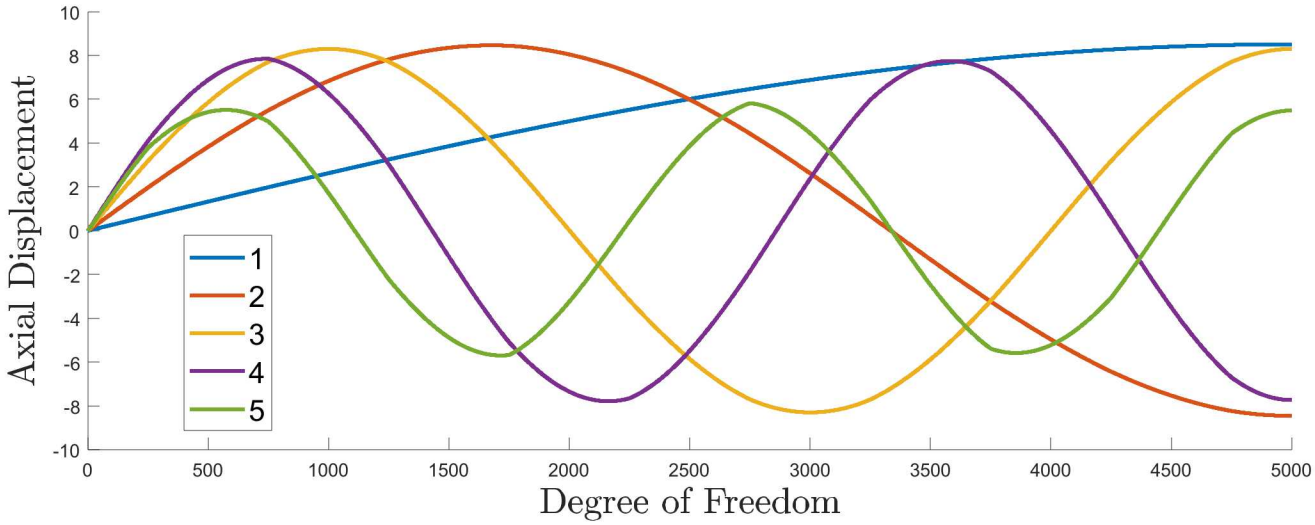

Figure 4. Plot of the first 5 mass-normalized mode shapes of the FEM under fixed-free conditions. The first 5 natural frequencies are 4.37, 8.71, 12.91, 16.62, 18.72 kHz.

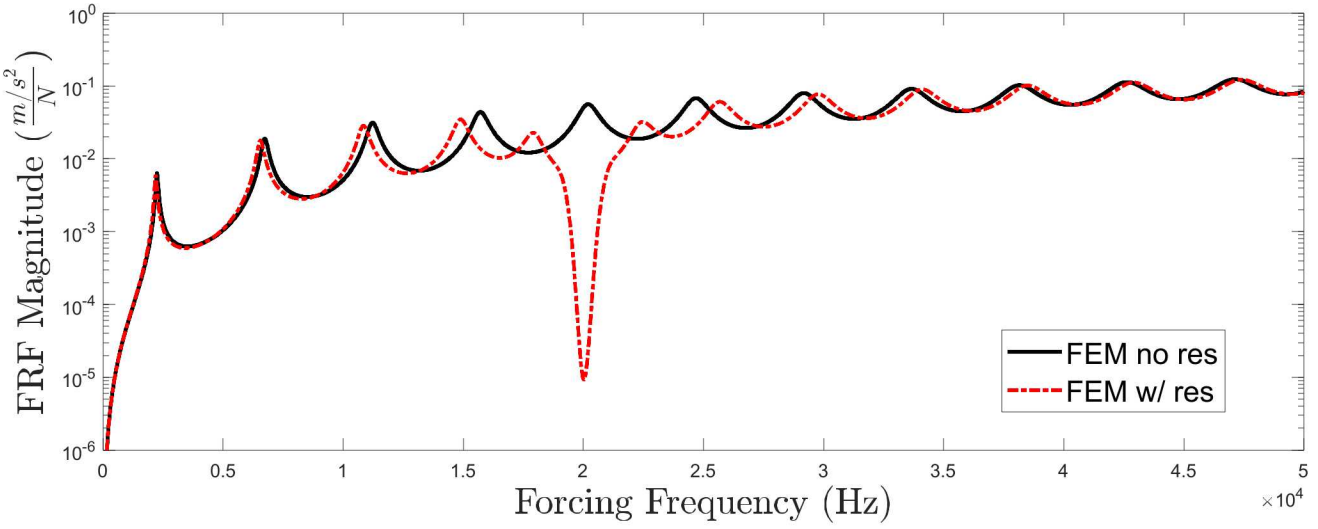

Figure 5. Plot of the FRF (left-end input, right-end output) of the metamaterial FEM for fixed-free conditions with and without the metaresonators attached.

It can be clearly seen from the FRF that there exists a dramatic lack of response in the region near 20 kHz, demonstrating the unique characteristic of metamaterial structures. The metaresonators act similarly to tuned mass dampers in that they absorb the kinetic energy of the parent structure's vibrational response at frequencies near their natural frequency, and if that natural frequency is near to a resonant frequency of the structure, the resonance peak is split.

3.2 Cell-Level Boundary Conditions

As discussed earlier, the Craig-Bampton method requires determination of the fixed-interface modes prior to synthesizing the components/cells to form the reduced assembly. This can be interpreted as the unit cell and its copies having fixed boundary conditions at the active DOFs. When using Guyan or SEREP reduction in performing the technique presented here, it is not initially apparent what, if any, boundary conditions should be assumed on the unit cell prior to copying and assembling. Apropos, a study is conducted pertaining to the effects of the unit cell's boundary conditions before being combined to the system-level reduced space, and the results are presented in **Tables 1-3**. Implementation of the boundary conditions is accomplished by attaching springs to left and right-end DOFs at the component level. A spring constant of $10^{-12}\ N/m$ is used to simulate a free condition, whereas a stiffness of $10^{12}\ N/m$ is used to simulate a fixed condition. For each run, the same DOFs were used as the active sets for the SEREP and Guyan reductions, in which 96% of the original FEM DOFs were deleted.

Table 1. Comparison of cell B.C.'s effects on the FRF prior to assembly when the FEM has free-free conditions.

Left B.C. (cell)	Right B.C. (cell)	SEREP FRAC	Guyan FRAC	Impr. Guyan FRAC
Free	Free	0.9505	0.4458	0.6330
Fixed	Free	0.0082	0.0078	0.0682
Fixed	Fixed	0.0174	0.0118	0.0159

Table 2. Comparison of cell B.C.'s effects on the FRF prior to assembly when the FEM has fixed-free conditions.

Left B.C. (cell)	Right B.C. (cell)	SEREP FRAC	Guyan FRAC	Impr. Guyan FRAC
Free	Free	0.9533	0.7081	0.7564
Fixed	Free	0.0198	0.1910	0.0327
Fixed	Fixed	0.2221	0.0131	0.1872

Table 3. Comparison of cell B.C.'s effects on the FRF prior to assembly when the FEM has fixed-fixed conditions.

Left B.C. (cell)	Right B.C. (cell)	SEREP FRAC	Guyan FRAC	Impr. Guyan FRAC
Free	Free	0.8763	0.6654	0.6677
Fixed	Free	0.0345	0.0270	0.3531
Fixed	Fixed	0.3263	0.1169	0.1059

For each scenario, it is apparent that using free-free conditions on the cells provides the most accurate FRF in the reduced assembly. That is, the entries in stiffness matrices pertaining to the left and right ends of the cells should not be adjusted to increase their rigidity. When using cell B.C.'s that are free-free, SEREP has great accuracy for system-level B.C.'s of free-free and fixed-free, but its accuracy noticeably suffers when reducing a fixed-fixed FEM. On the other hand, Guyan is best (though still lackluster) in reducing FEMs with fixed-free conditions, and suffers accuracy when the assembly B.C.'s are otherwise. Succinctly put, both methods are best-suited for the model reduction of FEMs with fixed-free conditions at the system level.

3.3 Variance in Reduction Percentage

To demonstrate the accuracy of each reduction method, FRF overlays are presented to visually compare the dynamic responses of the reduced-order models as the number of DOFs included in the active set decreases (i.e. the model is further reduced). The plots of the reduced models are named in reference to their cost savings quantified by *percent reduction*—the percentage of

cell DOF that were removed in the reduction process. Each graph also contains the FRF of the original FEM. In addition, a table is presented for each method to provide the FRACs associated with each curve.

Fig. 6 provides examples of the DOF selections for the reduction techniques used. For the Guyan and SEREP methods, the a-set DOFs must at minimum include the boundary nodes as well as the central DOF. Inclusion of more degrees of freedom in the reduced set requires selection of DOFs symmetrically about the center. It should be noted that the center DOF must be included even if the resonator is attached eccentrically (i.e., attached to the center DOF); the node where the resonator attaches is not as pertinent in this case. For Craig-Bampton reduction, only the boundary nodes are selected; the quality of the reduction is determined by the number of modes chosen to use at the component level (see **Eq. 19**). For the model presented here, there are three unique component/boundary types used: left-end, where the boundary set includes the right-most DOF; right-end, where the boundary set includes the left-most DOF; and interior, where the b-set includes both the left and right-most nodes.

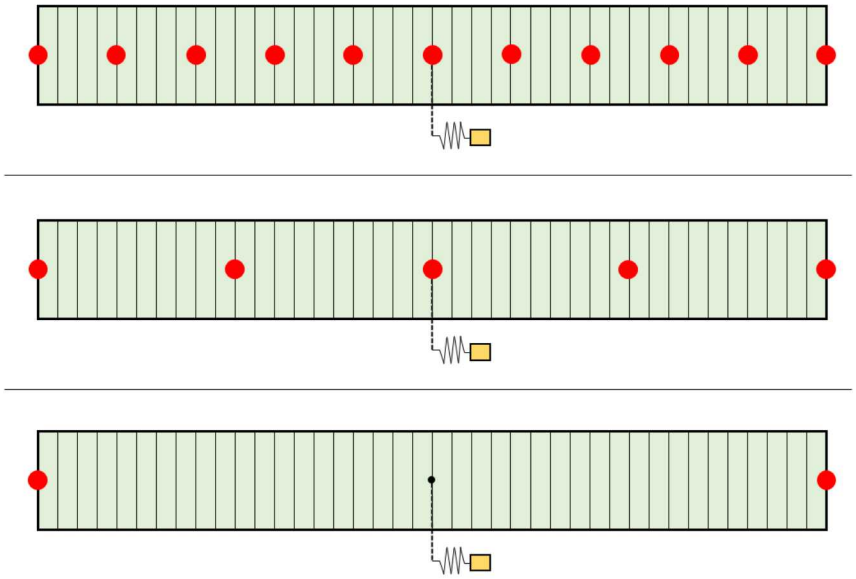

Figure 6. Diagram to provide examples of the a-set DOF selection pattern for the different reduction methods. (Top and center) A pattern which is symmetric about the center of the bar should be chosen for Guyan and SEREP. (Bottom) Only the interface DOFs are chosen for Craig-Bampton.

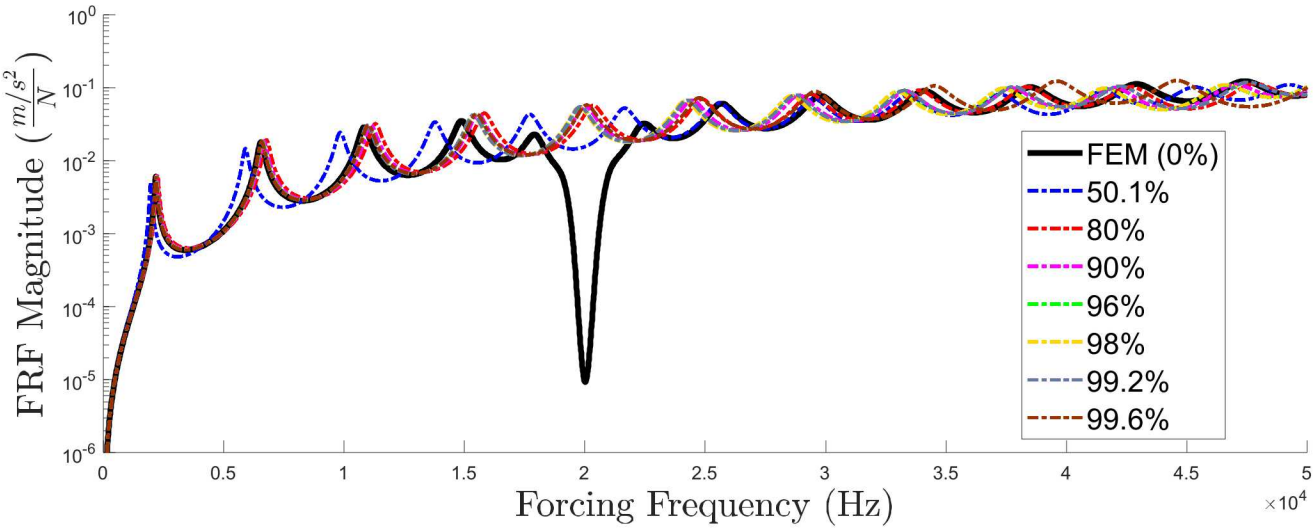

Figure 7. FRF overlays between the FEM and the Guyan ROM with varying percent reduction.

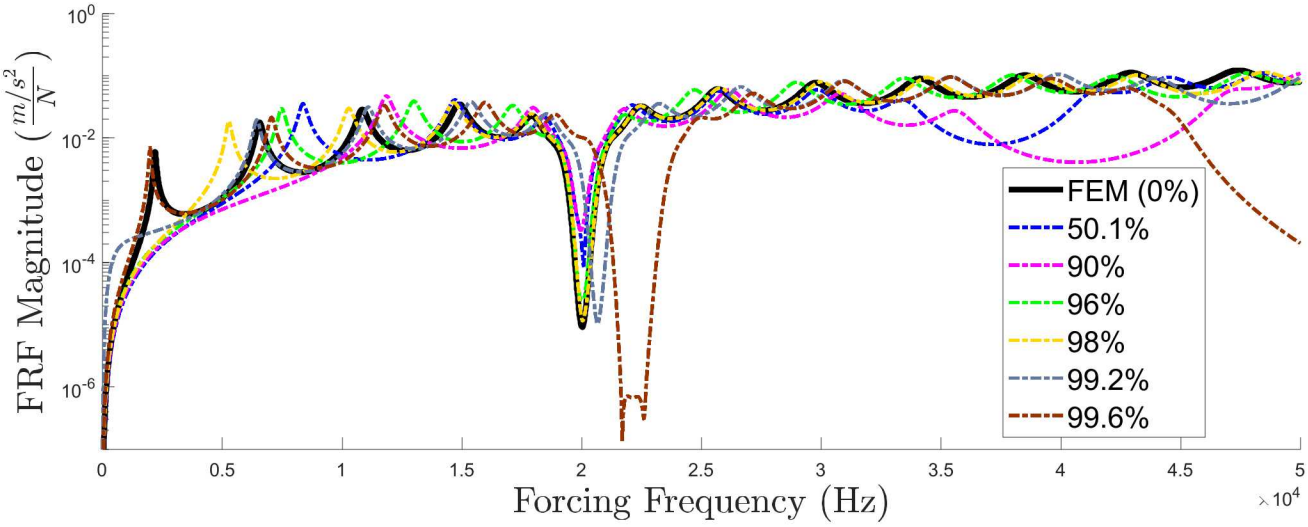

Figure 8. FRF overlays comparing the FEM and improved Guyan ROM with varying percent reduction.

Table 4. FRACs from Guyan condensation in relation to percent reduction.

Percent Reduction	Guyan FRAC	Impr. Guyan FRAC
50.1%	0.5745	0.5085
90%	0.7666	0.1824
96%	0.7081	0.7564
98%	0.6995	0.8791
99.2%	0.7122	0.6051
99.6%	0.3850	0.3326

The frequency responses of the traditional and improved Guyan reduction methods are compared in **Figs. 7-8**. It can be seen from **Fig. 7** that the standard Guyan condensation is overall ineffective for reduction of the metamaterial FEM. Most notably, the technique entirely neglects effects due to the metaresonators and predicts a response as though the resonators were not attached to the bar. This is due to the fact that the DOFs of the resonators where the masses reside must be included in the deleted set for the technique to operate properly. As a result, the masses of the resonators (and therefore their dynamic effects on the bar) are excluded in the Guyan condensation.

Fig. 8 shows that the improved Guyan method does account for the metaresonators quite well as a result of the augmented transformation matrix accounting for mass-inertial effects of the metaresonators. However, the improved technique comes with an interesting caveat: the results do not improve by including more DOFs in the active set. Rather, there appears to be a strong preference to certain a-set DOF distributions over others, regardless of the number of DOF retained. This is interesting because it is generally expected for lesser degrees of reduction to be more accurate than higher degrees. Also of note is that most of the ROM FRFs do not capture the first peak as in the FEM FRF.

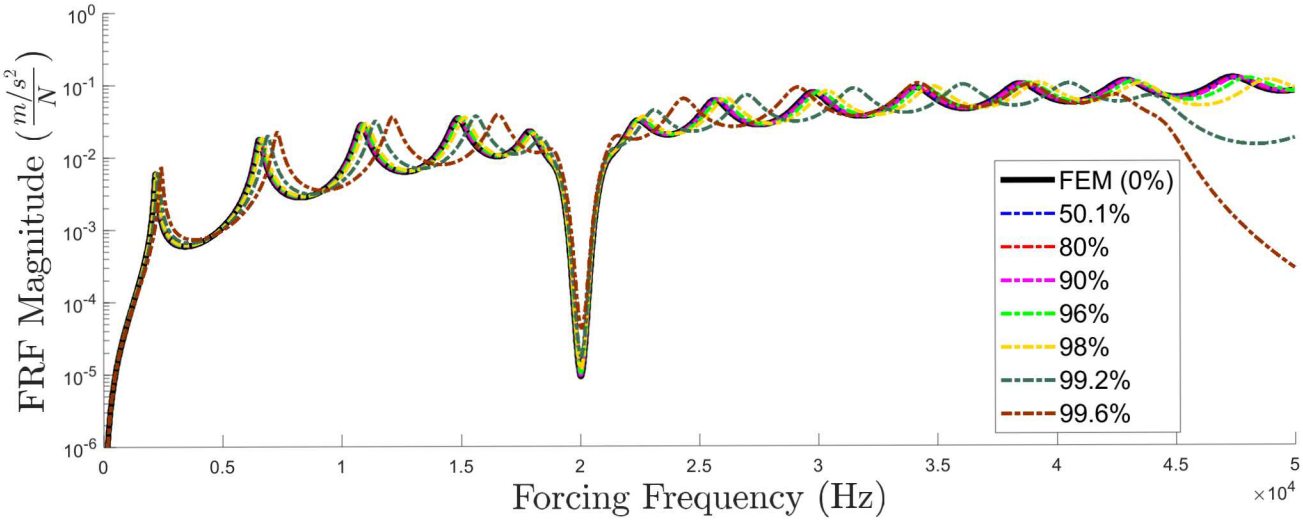

Figure 9. FRF overlays comparing the FEM and SEREP ROM with varying percent reduction.

Table 5. FRACs from the SEREP technique in relation to percent reduction.

Percent Reduction	SEREP FRAC
50.1%	0.9998
80%	0.9984
90%	0.9931
96%	0.8198
98%	0.6110
99.2%	0.4821
99.6%	0.4399

The results from the SEREP ROM are shown in **Fig. 9**. Overall, SEREP has good accuracy for reduction percentages of 96% and below. Considerable deviations from the finite element response only occur beyond 99% reduction. Interestingly, the SEREP ROM is extremely sensitive to the DOFs selected for the reduced set. For the model used here, the set of active DOFs is required to be symmetric about the location where the resonator attaches to the cell to obtain a reasonable solution. It can be seen from **Table 5** that SEREP offers exceptional accuracy for up to 90% reduction. However, the authors believe this is an oddity particular to this model, as this issue is not usually present when using the SEREP technique. It is likely due to the nature of the mode shapes of the unit cells being symmetric, thereby creating numerical issues with non-symmetric active DOF selection. In general, SEREP is more sensitive to the modes in U_a than the DOF locations/distributions.

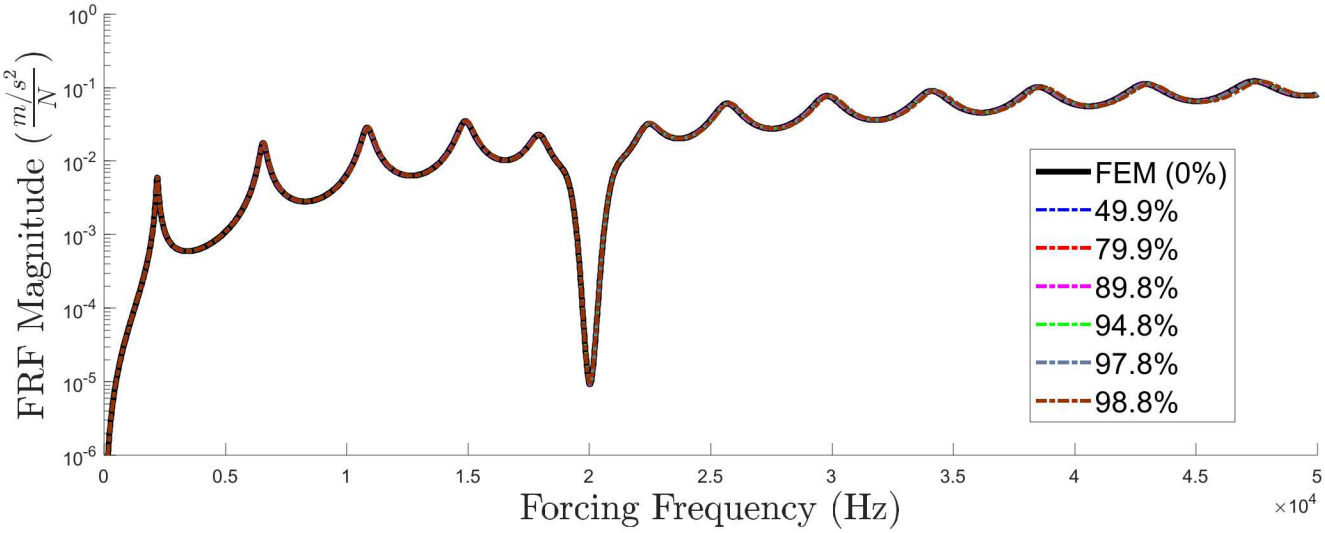

Figure 10. FRF overlays comparing the FEM and Craig-Bampton ROM with varying percent reduction.

Table 6. FRACs from the Craig-Bampton method in relation to percent reduction.

Percent Reduction	CBR FRAC
49.9%	1.0
79.9%	1.0
89.8%	0.9999
94.8%	0.9997
97.8%	0.9978
98.8%	0.9882

The results of the analysis pertaining to the Craig-Bampton method are shown in **Fig. 10**. It can be seen that CBR provides excellent accuracy in the dynamic response of the metamaterial bar even for considerably large reduction percentages. The FRAC values shown in **Table 6** show that even at nearly a 99% reduction, the accuracy of the frequency response suffers less than 1.2% error.

The primary reason why the solution accuracies begin to suffer for high percent reductions is due to the number of degrees of freedom in the cells being too few to accurately contain information on a sufficient number of modes. Single-mode FRF plots (i.e., plotting the resonant response of one mode at a time) are presented in **Fig. 11** to demonstrate the phenomenon using the SEREP method. The left plot represents the 90% reduced-order SEREP model. It can be seen that each single-mode FRF curve lines up appreciably well their corresponding resonance peaks in the FRF of the FEM. On the right plot, however, it can be seen that, at 99.6% reduction, SEREP does not contain sufficient information to accurately describe each resonance peak, and the solution accuracy suffers as a result. To improve results, more or better a-set DOF and modes would need to be selected. As SEREP is a modal filter of sorts, the choice of modes in the U_a matrix must be similar to the modes important to the response in order to accurately reduce the model.

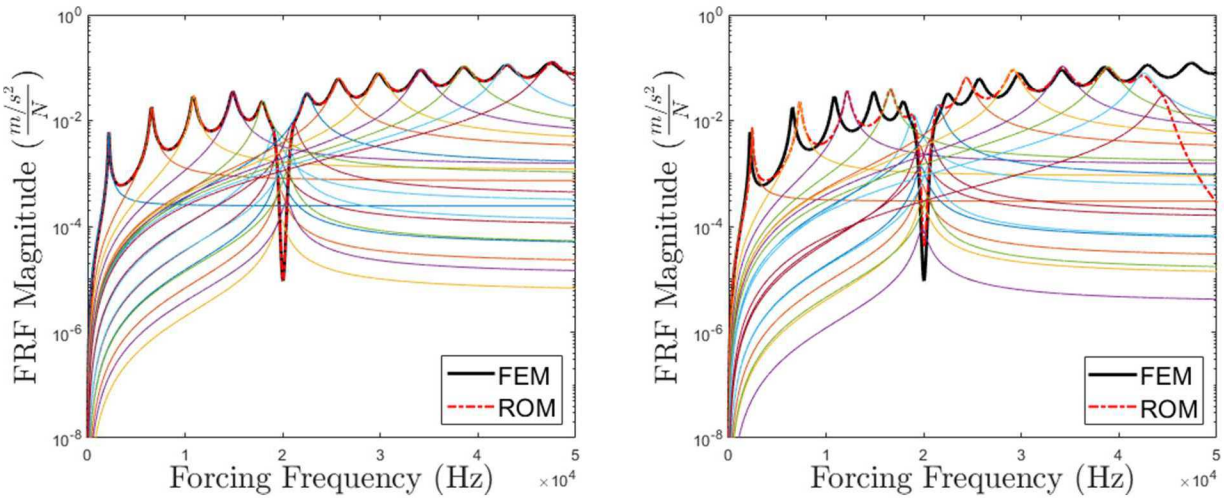

Figure 11. Single-mode FRF overlays of (left) 90% reduction and (right) 99.6% reduction. The SEREP technique is used for both plots.

3.4 Discussion of the Reduction Techniques

Numerous commercial finite element packages allow for reduced-order modeling using standard Guyan condensation and/or Craig-Bampton reduction. CBR provides an excellent means for model reduction and boasts the highest accuracy for this FEM. Considerably large degree of freedom reductions of nearly 99% can be applied and still yield excellent agreement with the original finite element model. However, Craig-Bampton reduction is notably more difficult to implement than typical model reduction techniques.

From the analysis presented here, it has been shown that Guyan reduction is inadequate for the reduction of this metamaterial model, because it entirely disregards the mass effects from the metaresonators. This may be due to the metaresonators being modeled as a simple spring-mass. Using the improved Guyan technique rectifies the issue; however, the accuracy of the improved solution is volatile depending on the amount of reduction applied. Despite these flaws, Guyan condensation is less arduous to implement than the Craig-Bampton method, and can lead to respectable accuracies under the proper conditions.

Less ubiquitous than its counterparts presented here, the SEREP technique is the fastest and least difficult method to implement for the presented model. The method is able to produce highly accurate reduced-order models of reduction percentages up to 90%. However, the selection of a-set degrees of freedom and modes in the U_a matrix is perhaps most critical for SEREP and can be a hindrance to obtaining an acceptable solution.

4 Conclusions

A finite element model of a simple metamaterial axial bar was developed to demonstrate how model reduction techniques can be used to reduce the computational cost of simulating metamaterial dynamics. The cost savings comes from taking advantage of the self-repeating structure of many metamaterials, where the system is comprised of multiple identical unit cells. Reduction of the unit cell can be performed with any of the various model reductions methods.

However, as shown in this work, the accuracy of the assembled system is affected by the reduction method as well as each methods' nuances. Interestingly, for the model used here, traditional Guyan reduction was ineffective because the static condensation does not account for the resonator mass effects, while Improved Guyan yielded better results. In general, Craig-Bampton or SEREP reduction methods provided good matches to the full FEM FRFs, although SEREP was sensitive to the choice of a-set DOF and modes.

The next step in this work will be to implement this ROM method on a three-dimensional model of a more geometrically complicated metamaterial. Lessons learned from this work, in terms of reduction methods and sensitivities, will be useful for developing the ROMs of the 3-D model. Likely, the main challenge with implementing this ROM method to a self-repeating three-dimensional model will be in the bookkeeping—keeping track of the cell-level interface DOF and making proper connections between the reduced cell DOF during the system assembly process.

References

[1] C. Nonis, L. Thibault, T. Marinone and P. Avitabile, "Development of Full Space System Model Modes from Expansion of Reduced Order Component Modal Information," in *Topics in Modal Analysis, Volume 7*, New York, NY, 2014.

[2] K. H. Matlack, A. Bauhofer, S. Krödel, A. Palermo and C. Daraio, "Composite 3D-Printed Metastructures for Low-Frequency and Broadband Vibration Absorption," in *Proceedings of the National Academy of Sciences*, 2016.

[3] R. J. Guyan, "Reudction of Stiffness and Mass Matrices," *AIAA Journal,* pp. Vol. 3, No. 2, pp. 380, 1965.

[4] P. Avitabile, "Model Reduction and Model Expansion and Their Applications Part 1 - Theory," Modal Analysis and Controls Laboratory, University of Massachusetts Lowell, 2005.

[5] R. R. Craig and A. J. Kurdila, Fundamentals of Structural Dynamics, Hoboken, NJ: John Wiley & Sons, Inc, 2006.

[6] P. Avitabile, "Test-Analysis Correlation-Updating Considerations," Modal Analysis and Controls Laboratory, University of Massachusetts Lowell.